All-fiber Sixth Harmonic Generation of Deep UV

YUN WANG,[1,*] TIMOTHY LEE,[1] FRANCESCO DE LUCIA,[1] MUHAMMAD I.M. ABDUL KHUDUS,[1,2] PIER J.A. SAZIO, [1] MARTYNAS BERESNA,[1] GILBERTO BRAMBILLA[1]

[1]*Optoelectronics Research Centre, University of Southampton, Southampton, SO17 1BJ United Kingdom*
[2]*Photonics Research Centre, Department of Physics, Faculty of Science, University of Malaya,50603 Kuala Lumpur, Malaysia*
**Corresponding author: yw11e13@soton.ac.uk*

Received XX Month XXXX; revised XX Month, XXXX; accepted XX Month XXXX; posted XX Month XXXX (Doc. ID XXXXX); published XX Month XXXX

We simulate and experimentally demonstrate deep UV generation from a 1550 nm laser source in a fully fiberized system by cascading second and third harmonic generation using a periodically poled silica fiber and an optical sub-micron diameter fiber. Harmonic generation is achieved by harnessing intermodal phase matching in optical microfibers and a permanent $\chi^{(2)}$ induced via thermal poling. As a result, efficient non-linear processes can be observed despite the low third-order nonlinear susceptibility of silica glass.

OCIS codes: *(060.4370) Nonlinear optics, fibers; (190.4160) Multiharmonic generation; (190.4410); Nonlinear optics, parametric processes; (230.1150) All-optical devices.*

http://dx.doi.org

Ultraviolet (UV) light has numerous applications ranging from medical disinfection and food manufacturing to high-resolution lithography [1-3]. At present, generation of UV is mostly achieved with gas lasers or diodes, or relies on nonlinear processes which enable frequency conversion from long wavelengths. Cascaded frequency conversion into the deep-UV (i.e. at wavelengths of λ<300nm) generally exploits nonlinear crystals, such as beta barium borate, or a hybrid of bulk and fiber systems [4-5]. Broadband supercontinuum generation covering the UV has been reported using photonic crystal fibers through mechanisms such as self-phase modulation, soliton generation and four wave mixing [6-7]. The use of fibers provides the advantage of long interaction lengths with a well confined and controlled intensity profile, and using silica fibers highly transparent in the UV also avoids thermal effects, which needs to be handled carefully for crystals such as beta barium borate [8].

In this paper, deep UV generation is demonstrated by cascading second harmonic (SH) and third harmonic generation (THG), where the former was generated from a high power 1550 nm laser source which is frequency doubled by means of a periodically poled silica fiber (PPSF) and then employed as the pump source for the latter, generated in a sub-micron diameter optical fiber taper.

Despite lacking any significant second-order nonlinearity $\chi^{(2)}$ and exhibiting a small third-order nonlinear susceptibility, efficient harmonic generation in silica glass has been demonstrated using poling and intermodal phase matching [9-14]. A permanent $\chi^{(2)}$ can be generated via the thermal poling process [9], where a heated glass (~250°C–300°C) immersed in an electric field experiences a redistribution of the impurity charge carriers, resulting in the formation of a space-charge region located near the anode. After cooling the glass in the presence of the electric field, a permanent $\chi^{(2)} \sim 3\chi^{(3)}E_{rec}$ is created as consequence of a third order nonlinear optical rectification process, where E_{rec} refers to the (recorded) electric field permanently frozen inside the space-charge region of the poled glass [10]. The electric field is typically introduced in the fiber sample by connecting a high anodic potential to wires manually inserted or molten metal filled into twin-hole structures [11]. The PPSF used here is a twin-hole fused silica Ge-doped core optical fiber. Liquid electrodes have been used for facile removal, low loss and enhanced sample length [12]. In order to fulfil the phase-velocity matching condition between pump and SH, the thermal poling process has been followed by a periodic erasure of the frozen-in electric field using UV light to achieve quasi-phase matching [13-14].

Certain nonlinear phase-matched parametric processes such as harmonic generation can also be achieved using optical microfibers (OMF), and here we use it for THG. In an OMF, dispersion can be tailored by optimizing the fiber taper diameter to meet the phase matching condition between the pump fundamental mode and a harmonic higher-order mode, which experience a large modal overlap with each other. Simultaneously, the diffraction-limited confinement in OMFs leads to high pump intensities resulting in an efficient conversion. Conversion from the near infrared to the visible and the near UV has been previously demonstrated experimentally via THG [15] and four-wave-mixing [16], respectively.

The theoretical OMF diameters for phase matching the pump (i.e. SH output from PPSF) with its third harmonic in the deep-UV were obtained by solving rigorous modal eigenvalue equations for an air-clad and silica-core fiber [17]. The effective index dependence on the air-clad OMF diameter is plotted in Fig.1(a) with each intersection point corresponding to a phase matching diameter

(PMD). To select the most suitable mode for THG, the modal overlap integral J_3 was evaluated [18] for the different modes at each PMD:

$$J_3 = \oiint_{A_{silica}} (F_1^* \cdot F_3)(F_1^* \cdot F_1^*)\, dS \qquad (1)$$

where F_1 and F_3 are the normalized electric field distributions of the pump fundamental and harmonic higher modes respectively. As expected from modal symmetry, the harmonic HE_{12} mode has the best overlap with the fundamental HE_{11} mode. We therefore aim to phase match these 2 modes by fabricating a microfiber diameter close to their PMD of 344nm for sixth harmonic (6H) generation, i.e., producing the third harmonic of the second harmonic at λ_{SH}~775 nm from the PPSF (Fig.1(b)).

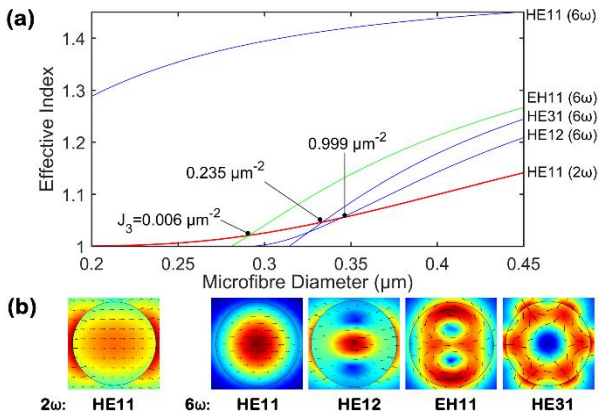

Fig. 1. (a) Dependence of the effective index on the air-clad OMF diameter for the SH fundamental mode at λ=775 nm and 6H high-order modes at λ=258 nm. The values of the modal overlap integral J_3 for each PMD are labelled for reference. (b) Modal field |E| distribution for SH fundamental and 6H higher order modes.

The conversion efficiency was simulated using equations derived by Grubsky and Savchenko [18], where phase mismatches associated to cross and self-phase modulation were compensated by optimizing the detuning term which later is physically achieved by detuning the optimized diameter. As most silica-related defects exhibit absorption in the UV [19], the attenuation of the fiber used in the OMF fabrication was characterized via the cut-back method, resulting in a loss of α= 0.09 dB/cm at λ=258 nm, which was then used in the simulations. Conversion efficiencies >50% are predicted in a 3cm-long OMF at a pump peak power of 200 W (Fig. 2).

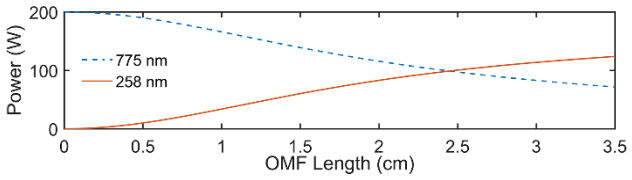

Fig. 2. Simulated conversion for 6H generation, i.e., the third harmonic generation from λ=775 nm, as a function of the OMF length.

The fundamental frequency signal for the experiment was generated from a master oscillator power amplifier (MOPA) operating at λ~1550 nm [16] and spliced to the PPSF to avoid connector-induced coupling losses (Fig. 3). The pulse duration and repetition rate of the MOPA were 4ns and 200kHz, respectively.

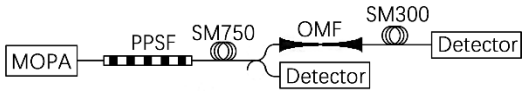

Fig. 3. Schematic of the setup for 6H generation and detection.

Before being spliced to the system, the PPSF was characterized using the seed source of the MOPA, a tunable ~1.55μm continuous-wave laser (Photonetics Tunics BT). The PPSF spectral response was measured by sweeping the wavelength of the source while simultaneously monitoring the PPSF output using a power meter (Thorlabs S130VC), indicating a PPSF working bandwidth of 1.25nm. Power measurements (Fig. 4(a)) confirm a square dependence of the output power on the input power and suggests a conversion efficiency of 1.56×10^{-2} %/W for this 30 cm long PPSF. The light source was then replaced with the MOPA. By measuring the input and output pump powers and the output harmonic power, and assuming a harmonic splicing loss similar to the 0.85 dB loss recorded at the pump wavelength, characterization using the low power continuous wave seed source as well as the high power pulsed MOPA both suggested a $\chi^{(2)}$ of 0.04 pm/V for the PPSF used here. Although $\chi^{(2)}$ is somewhat smaller than previously published values [12], the relatively large operational bandwidth allows the system to operate without a temperature controller, which is otherwise recommended. The output spectrum was monitored using a spectrum analyzer (Yokogawa AQ6370) for the infrared and visible, spectrometers (Ocean Optics USB Series) for the visible and the UV and a coupler with attenuation of around -20dB and -10dB at the fundamental and the harmonic, respectively. The SH signal-to-noise ratio and linewidth were estimated to be larger than 40 dB, and ~0.03nm, respectively (Fig. 4(b)). No nonlinear broadening or output in different spectral regions was observed.

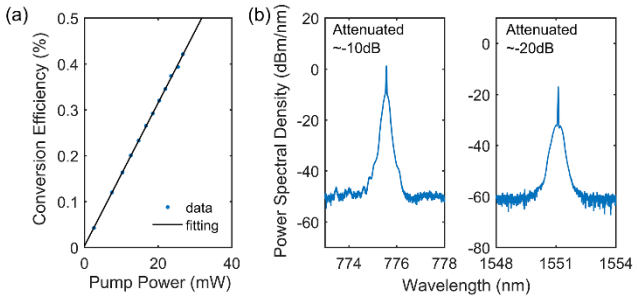

Fig. 4. (a) Conversion efficiency for the 30 cm long PPSF. (b) SH and pump spectra measured at PPSF output attenuated using a tap coupler.

A single-mode fiber with a cut-off wavelength below 750 nm (Fibercore SM750) was spliced to the PPSF output before the tap coupler (Fig. 3) to minimize the 1550nm pump residue, which could otherwise saturate or damage the spectrometer. The coupler was changed to a tap coupler (-20dB at 775 nm) for real-time monitoring and optimization of the PPSF efficiency by varying a polarizer close to the end of the MOPA system. Similarly, a short piece of single-mode fiber with a cut-off wavelength below 310 nm (Thorlabs SM300) was spliced to the OMF output as a power delivery fiber. This fiber was employed to remove the SH signal at λ~775 nm to avoid saturating the spectrometer with background noise, and is also relatively transparent in the deep-UV as it does not present obvious material defect-induced absorption at around 250

nm, which might otherwise be detrimental for the observation of the generated 6H. To eliminate light scattered into the cladding at the splicing point, part of the SM300 had its polymer coating replaced with graphite glue and bent.

To reduce absorption in the UV, OMFs were fabricated from a submarine telecom fiber (Sumitomo) with a fluorine-doped cladding and a pure silica core - transparent in the UV except for the ODC-induced absorption band centered at λ~250 nm - and the SM300 was used for power collection. While pulling the fiber, the output spectrum was recorded in real time using a UV spectrometer (USB4000, Ocean Optics), and a deep-UV signal at λ~258.5 nm was clearly observed (Fig. 5). As pulling continued, the phase matching region shifted to different positions along the transition region, resulting in a long tail at the vanishing side of the peak in the time domain. Before and after the emergence of the 6H, signals at λ~387.5 nm were also observed. This is believed to be the fourth harmonic (4H), which is based on bulk multipole nonlinearities as well as surface dipole [19-20]. The theoretical PMDs for SH generation from a λ=775 nm pump are D=329 nm and 373 nm for power conversions into the harmonic TM_{01} and HE_{21} modes, respectively.

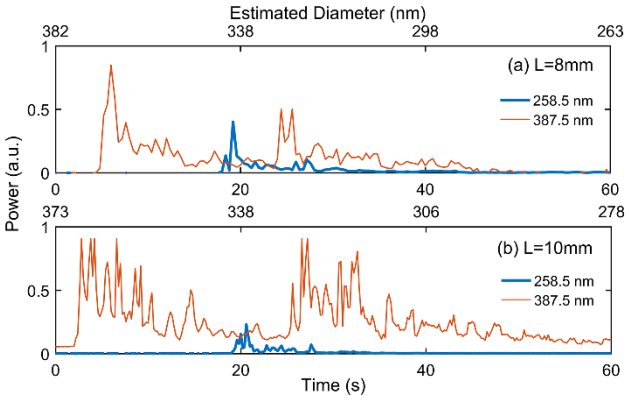

Fig. 5. 6H (258.5 nm) and 4H (387.5 nm) spectra for (a) an 8 mm and (b) a 10 mm-long microfiber recorded during fiber pulling. Note that the starting point of time axis is arbitrary.

While short tapers have low conversion efficiency, tapers with long transition regions are likely to have poor signal-to-noise ratios (Fig.5(b), for instance) due to the tail of the first 4H generated in the taper transition region and the movement of the holder for fiber pulling. Therefore, most microfibers were fabricated to have a waist length of 8mm.

To compare the PMD with the theoretical predictions, fiber pulling was manually stopped at the onset of the 6H for SEM imaging. Due to the high tapering temperature and thermal-optic effect ($dn/dT = 1.1 \times 10^{-5}$/°C for silica) the OMF diameter was found to be ~5 nm smaller than the PMD simulated for room temperature (Fig. 6).

Because of the thermally induced shift mentioned above, the 6H power dependence on the SH power was examined by terminating pulling at the onset of the deep-UV signal and varying a polarization controller before the PPFS to change its efficiency while monitoring a fraction of the output from the tap coupler, when the OMF was kept inside the microheater. The result shown in Fig. 7 suggests a 6H power dependence on the SH power close to the theoretical cubic trend.

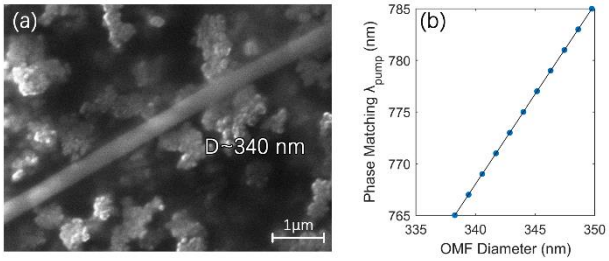

Fig. 6. (a) SEM image of the taper waist, and (b) the theoretical phase matched 2H wavelength against OMF diameter for 6H generation.

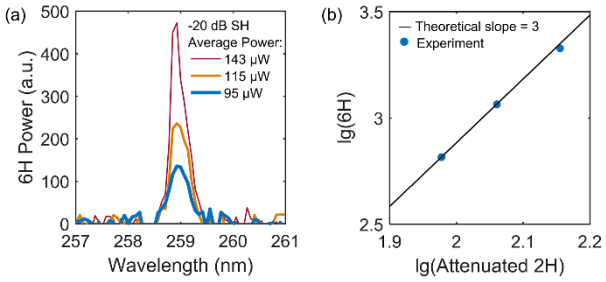

Fig. 7. (a) 6H spectra for different SH power, and (b) data processed from (a) showing the 6H power dependence on the 2H power.

To measure the maximum 6H power, pulling has to be terminated when fiber diameter reaches exactly the PMD; yet this is challenging due to the limited tunable SH wavelength range which implies that a diameter control precision smaller than 0.7nm is required (Fig. 6(b)). One of the possible solutions is to slow down the pulling speed and improve the software for pulling so it can be paused for repeating spectrum measurement at the room temperature for OMF diameters close to the PMD. Here the output spectrometer was replaced with a high-sensitivity power meter (Ophir PD300R-UV). The presence of the 6H was confirmed by monitoring the estimated diameter well as the three-peak profile given by both the 4Hs and 6H. Sweeping the OMF diameter and the detuning in the simulation suggests that around the point where efficiency is most sensitive to diameter, a change of 0.013 nm in diameter can cause a detuning of 300 m^{-1} which can halve the 6H power. The speed at which the OMF diameter decreased during tapering was estimated to be about 1.7nm/s around the PMD, which suggests that the peak power generated in the taper region lasts ~8 ms during pulling. As the power meter response time is 0.2 s, the power reading is averaged over this period and therefore over an order of magnitude less than the true experimental maximum value.

When the peak power at λ~775nm was 13 W, the average deep-UV 6H power recorded during pulling for an OMF length of 8mm was 0.15 nW after subtracting the background noise level of 0.15 nW induced by 775 nm residue (Fig.8), corresponding to a peak power of 0.18 μW. For comparison, by repeating the simulation for Fig. 2 using the experimental SH power, the theoretical prediction of the 6H power should have been 7mW.

During fiber pulling, the background power level arising from the SH residue at λ~775 nm was checked from the beginning to ensure that the fiber was straight. Besides the reduction in measured power related to the slow power meter response time, a difference of approximately two orders of magnitude in the conversion efficiency is attributable to microfiber surface roughness.

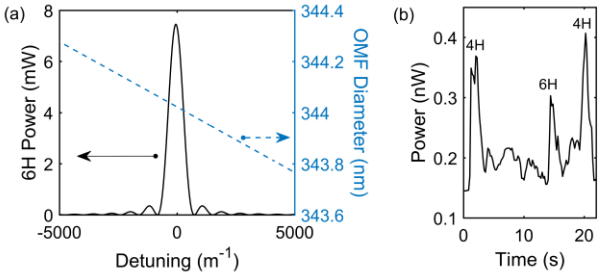

Fig. 8. (a) Simulated relationship between the OMF diameter, the 6H power and the detuning. (b) Power recorded during fiber puling. The power meter was calibrated for the 6H wavelength only.

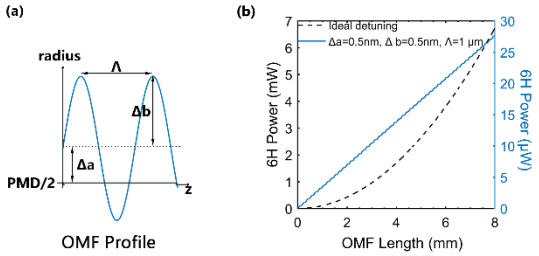

Fig. 9. (a) Radius profile of OMF with a surface wave, and (b) its impact on 6H conversion.

As the OMF is manufactured with a continuous molten glass reflow, the surface roughness is mostly associated to surface waves arising from fluctuations present at high temperature during fiber fabrication [22-23]. This was modelled and confirmed by approximating the OMF radius r(z) as a sinusoidal variation for the 6H generation from the SH here (Fig. 9). When both the radius deviation (Δa) and the fluctuation amplitude (Δb) are 0.5 nm and the period (Λ) is 1 μm, the theoretical 6H peak power reduces from 7 mW to below 30 μW, which is consistent with previous results [24]. Nevertheless, this can be improved by controlling the OMF radius uniformity to sub-nanometer precision by exploiting, for example, CO_2 lasers [25]. Moreover, optimizing PPSF efficiency and increasing PPSF and OMF lengths can also improve the overall efficiency. Therefore, under the best-case scenario, high efficiency for applications can still be expected.

In conclusion, the sixth harmonic generation of deep UV light from a λ=1550nm pump was simulated and experimentally demonstrated in a fully fiberized system. The temporal walk-off was minimized by using a nanosecond pulse laser as the pump. Material absorption in the UV was minimized by using fibers with F-doped claddings and pure silica cores. A power of 0.15 nW was recorded at a wavelength of 259nm and can be increased by orders of magnitude by improving pump source, measurement method and optimizing the OMF taper profile.

The data from this Letter can be obtained from the University of Southampton repository at: doi.org/10.5258/SOTON/D0192.

Funding. UK Engineering and Physical Sciences Research Council (EPSRC) EP/L01243X/1 and EP/I035307/1.

Acknowledgment. The author would like to thank Neil Sessions at the ORC for support in using public shared devices.

References

1. K. Song, M. Mohseni, and F. Taghipour, Water Res. **94**, 341 (2016).
2. T. Bintsis, E. Litopoulou-Tzanetaki, and R.K. Robinson, J. Sci. Food Agric. **80**, 637 (2000).
3. M. Han, W. Lee, S.K. Lee, and S.S. Lee, Sensors Actuators, A Phys. **111**, 14 (2004).
4. M. Yoshimura, Y. Takahashi, H. Adachi, and Y. Mori, in *Adv. Solid State Lasers* (Optical Society of America, 2014), p. ATu4A.1.
5. Y. Urata, T. Shinozaki, Y. Wada, Y. Kaneda, S. Wada, and S. Imai, Appl. Opt. **48**, 1668 (2009).
6. J.H. Kim, M.-K. Chen, C.-E. Yang, J. Lee, S.S. Yin, P. Ruffin, E. Edwards, C. Brantley, and C. Luo, Opt. Express **16**, 4085 (2008).
7. S.P. Stark, J.C. Travers, and P.S.J. Russell, Opt. Lett. **37**, 770 (2012).
8. E. Gabryte, S. Sobutas, M. Vengris, and R. Danielius, Appl. Phys. B Lasers Opt. **120**, 31 (2015).
9. R.A. Myers, N. Mukherjee, and S.R.J. Brueck, Opt. Lett. **16**, 1732 (1991).
10. P.G. Kazansky and P.S.J. Russel, Opt. Commun. **110**, 611 (1994).
11. W. Margulis, O. Tarasenko, and N. Myrén, Opt. Express **17**, 15534 (2009).
12. F. De Lucia, D.W. Keefer, C. Corbari, and P.J.A. Sazio, Opt. Lett. **42**, 69 (2017).
13. J.A. Armstrong, N. Bloembergen, J. Ducuing, and P.S. Pershan, Phys. Rev. **127**, 1918 (1962).
14. A. Canagasabey, C. Corbari, Z. Zhang, P.G. Kazansky, and M. Ibsen, Opt. Lett. **32**, 1863 (2007).
15. T. Lee, Y. Jung, C. a. Codemard, M. Ding, N.G.R. Broderick, and G. Brambilla, Opt. Express **20**, 8503 (2012)
16. M.I.M. Abdul Khudus, F. De Lucia, C. Corbari, T. Lee, P. Horak, P. Sazio, and G. Brambilla, Opt. Lett. **41**, 761 (2016).
17. A.W. Snyder and J.D. Love, *Optical Waveguide Theory* (Springer US, Boston, MA, 1984).
18. V. Grubsky and A. Savchenko, Opt. Express **13**, 6798 (2005).
19. R. Salh, in *Cryst. Silicon - Prop. Uses*, edited by S. Basu (InTech, 2011), pp. 135–172.
20. J. Lægsgaard, J. Opt. Soc. Am. B **27**, 1317 (2010).
21. M.A. Gouveia, T. Lee, R. Ismaeel, M. Ding, N.G.R. Broderick, C.M.B. Cordeiro, and G. Brambilla, Appl. Phys. Lett. **102**, (2013).
22. T. Seydel, M. Tolan, B.M. Ocko, O.H. Seeck, R. Weber, E. DiMasi, and W. Press, Phys. Rev. B - Condens. Matter Mater. Phys. **65**, 1842071 (2002).
23. J. Jackle and K. Kawasaki, J. Phys. Condens. Matter **7**, 4351 (1995).
24. M.I.M.A. Khudus, T. Lee, P. Horak, and G. Brambilla, Opt. Lett. **40**, 1318 (2015).
25. M. Sumetsky, D.J. DiGiovanni, Y. Dulashko, J.M. Fini, X. Liu, E.M. Monberg, and T.F. Taunay, Opt. Lett. **36**, 4824 (2011).

Full references (to aid the editor and reviewers)

1. K. Song, M. Mohseni, and F. Taghipour, "Application of ultraviolet light-emitting diodes (UV-LEDs) for water disinfection: A review," Water Res. **94**, 341–349 (2016).
2. T. Bintsis, E. Litopoulou-Tzanetaki, and R. K. Robinson, "Existing and potential applications of ultraviolet light in the food industry - A critical review," J. Sci. Food Agric. **80**, 637–645 (2000).
3. M. Han, W. Lee, S. K. Lee, and S. S. Lee, "3D microfabrication with inclined/rotated UV lithography," Sensors Actuators, A Phys. **111**, 14–20 (2004).
4. M. Yoshimura, Y. Takahashi, H. Adachi, and Y. Mori, "Nonlinear Crystals for Deep-UV Light Generation," in *Advanced Solid State Lasers*, OSA Technical Digest (online) (Optical Society of America, 2014), paper ATu4A.1.
5. Y. Urata, T. Shinozaki, Y. Wada, Y. Kaneda, S. Wada, and S. Imai, "Deep UV light generation by a fiber/bulk hybrid amplifier at 199 nm.," Appl. Opt. **48**, 1668–74 (2009).
6. J. H. Kim, M.-K. Chen, C.-E. Yang, J. Lee, S. S. Yin, P. Ruffin, E. Edwards, C. Brantley, and C. Luo, "Broadband IR supercontinuum generation using single crystal sapphire fibers," Opt. Express **16**, 4085 (2008).
7. S. P. Stark, J. C. Travers, and P. S. J. Russell, "Extreme supercontinuum generation to the deep UV," Opt. Lett. **37**, 770–772 (2012).
8. E. Gabryte, S. Sobutas, M. Vengris, and R. Danielius, "Control of thermal effects in fast-switching femtosecond UV laser system," Appl. Phys. B Lasers Opt. **120**, 31–39 (2015).
9. R. A. Myers, N. Mukherjee, and S. R. J. Brueck, "Large second-order nonlinearity in poled fused silica," Opt. Lett. **16**, 1732 (1991).
10. P. G. Kazansky and P. S. J. Russel, "Thermally poled glass: frozen-in electric field or oriented dipoles?," Opt. Commun. **110**, 611–614 (1994).
11. W. Margulis, O. Tarasenko, and N. Myrén, "Who needs a cathode? Creating a second-order nonlinearity by charging glass fiber with two anodes," Opt. Express **17**, 15534–15540 (2009).
12. F. De Lucia, D. W. Keefer, C. Corbari, and P. J. A. Sazio, "Thermal poling of silica optical fibers using liquid electrodes," Opt. Lett. **42**, 69 (2017).
13. J. A. Armstrong, N. Bloembergen, J. Ducuing, and P. S. Pershan, "Interactions between light waves in a nonlinear dielectric," Phys. Rev. **127**, 1918–1939 (1962).
14. A. Canagasabey, C. Corbari, Z. Zhang, P. G. Kazansky, and M. Ibsen, "Broadly tunable second-harmonic generation in periodically poled silica fibers.," Opt. Lett. **32**, 1863–1865 (2007).
15. T. Lee, Y. Jung, C. A. Codemard, M. Ding, N. G. R. Broderick, and G. Brambilla, "Broadband third harmonic generation in tapered silica fibres," Opt. Express **20**, 8503 (2012).
16. M. I. M. Abdul Khudus, F. De Lucia, C. Corbari, T. Lee, P. Horak, P. Sazio, and G. Brambilla, "Phase matched parametric amplification via four-wave mixing in optical microfibers," Opt. Lett. **41**, 761 (2016).
17. A. W. Snyder and J. D. Love, *Optical Waveguide Theory* (Springer US, 1984).
18. V. Grubsky and A. Savchenko, "Glass micro-fibers for efficient third harmonic generation.," Opt. Express **13**, 6798–6806 (2005).
19. R. Salh, "Defect Related Luminescence in Silicon Dioxide Network: A Review," in *Crystalline Silicon - Properties and Uses*, S. Basu, ed. (InTech, 2011), pp. 135–172.
20. J. Lægsgaard, "Theory of surface second-harmonic generation in silica nanowires," J. Opt. Soc. Am. B **27**, 1317 (2010).
21. M. A. Gouveia, T. Lee, R. Ismaeel, M. Ding, N. G. R. Broderick, C. M. B. Cordeiro, and G. Brambilla, "Second harmonic generation and enhancement in microfibers and loop resonators," Appl. Phys. Lett. **102**, (2013).
22. T. Seydel, M. Tolan, B. M. Ocko, O. H. Seeck, R. Weber, E. DiMasi, and W. Press, "Freezing of capillary waves at the glass transition," Phys. Rev. B - Condens. Matter Mater. Phys. **65**, 1842071–1842077 (2002).
23. J. Jackle and K. Kawasaki, "Intrinsic roughness of glass surfaces," J. Phys. Condens. Matter **7**, 4351–4358 (1995).
24. M. I. M. A. Khudus, T. Lee, P. Horak, and G. Brambilla, "Effect of intrinsic surface roughness on the efficiency of intermodal phase matching in silica optical nanofibers," Opt. Lett. **40**, 1318–1321 (2015).
25. M. Sumetsky, D. J. DiGiovanni, Y. Dulashko, J. M. Fini, X. Liu, E. M. Monberg, and T. F. Taunay, "Surface nanoscale axial photonics: robust fabrication of high-quality-factor microresonators," Opt. Lett. **36**, 4824 (2011).